IEEE Access
Multidisciplinary | Rapid Review | Open Access Journal

Received February 8, 2019, accepted March 2, 2019, date of publication March 18, 2019, date of current version April 1, 2019.

Digital Object Identifier 10.1109/ACCESS.2019.2904327

A Novel Approach to the Optimization of a Solid Oxide Fuel Cell Anode Using Evolutionary Algorithms

SZYMON BUCHANIEC[1], ANNA SCIAZKO[1,2], MARCIN MOZDZIERZ[1], AND GRZEGORZ BRUS[1]

[1]Department of Fundamental Research in Energy Engineering, AGH University of Science and Technology, 30-059 Kraków, Poland
[2]Institute of Industrial Science, The University of Tokyo, Tokyo 153-0041, Japan

Corresponding author: Grzegorz Brus (brus@agh.edu.pl)

This work was supported by the Foundation for Polish Science under FIRST TEAM program No. First TEAM/2016-1/3 co-financed by the European Union under the European Regional Development Fund.

ABSTRACT Solid oxide fuel cell (SOFC) has a high energy conversion efficiency and emits a low level of pollutants in the environment. One of the crucial elements is an anode that, typically, is a composite of nickel and yttria-stabilized zirconia (Ni-YSZ). The microstructure morphology of an anode plays an important role in determining the electrochemical performances of a single cell and, consequently, a stack of cells. Therefore, the microstructure optimization design should be included in the development of a system at a very early stage. The anode material microstructure can be tailored to fulfill the role it has at the particular location in the stack. This paper presents a novel approach of using an evolutionary algorithm to optimize the microstructure of an SOFC's anode. The optimization problem consists of 16 microstructural parameters connected by the mesh of the dependencies. One group of algorithms that can face this challenge is an evolutionary algorithm family. In this paper, a genetic algorithm and a particle swarm optimization are employed to optimize the cell microstructure and to help in improving the performance of an SOFC. The developed mathematical model can correctly predict the performance of the SOFC anode and is employed in the evolutionary algorithms to select the optimal microstructure. The results show that the optimal microstructure leads to better cell performance than the conventional one.

INDEX TERMS Anodes, evolutionary computation, fuel cells, genetic algorithms, microstructure, particle swarm optimization, solid oxide fuel cell, optimization, energy conversion.

I. INTRODUCTION

A. SOLID OXIDE FUEL CELLS

A Solid Oxide Fuel Cell (SOFC) is an electrochemical device that converts the chemical energy of fuels directly into electricity. SOFCs have high energy conversion efficiency in a wide range of power output, which is graphically presented in Fig. 1. A typical solid oxide fuel cell consists of two porous ceramic electrodes (the cathode and the anode) separated by a solid, dense ceramic electrolyte made typically of yttria-stabilized zirconia (YSZ). An effective anode material allows electrochemical reactions in a large fraction of the volume of the electrode. The most common SOFC anode is a porous Ni/YSZ cermet. Each phase plays a unique and essential role in the transport phenomena providing pathways for different species: the YSZ phase for oxygen ions, the Ni phase for electrons and the pore phase for gases. As a consequence, the electrochemical reaction occurs only at the boundary of the three phases, the so-called Triple Phase Boundary (TPB). This contiguous contact of electronic, ionic and gas phases provides a direct link between the microstructure and the electrochemical performance of the anode. Figure 2 presents the role of each phase in the transport of charge and mass in the vicinity of the reaction domain in a conventional Ni/YSZ anode. The diffusion of oxygen ions from the cathode to the anode through the electrolyte is the slowest transport process. Consequently, electrochemical reactions occur in the vicinity of the anode-electrolyte interface.

B. SOFC MICROSTRUCTURE DESIGN

The breakthrough in microstructure design came together with the development of direct microstructure observation methods. For example, the FIB-SEM electron tomography. The FIB-SEM combines a Focused Ion Beam (FIB) and

The associate editor coordinating the review of this manuscript and approving it for publication was Rui Xiong.

2169-3536 © 2019 IEEE. Translations and content mining are permitted for academic research only.
Personal use is also permitted, but republication/redistribution requires IEEE permission.
See http://www.ieee.org/publications_standards/publications/rights/index.html for more information.

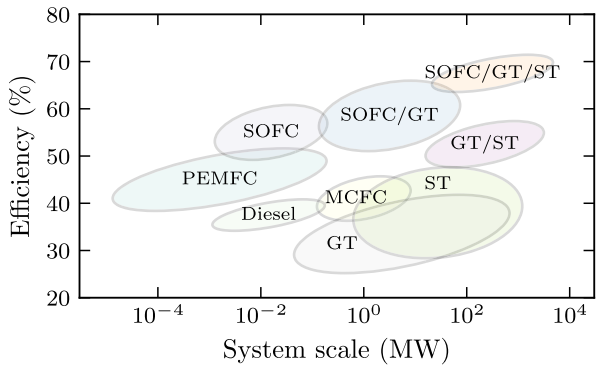

FIGURE 1. SOFC efficiency compared to other technologies in a wide range of power output [1]–[5]. GT - gas turbine, ST - steam turbine, MCFC - Molten Carbonate Fuel Cell, PEMFC - Proton-exchange Membrane Fuel Cell, SOFC - Solid Oxide Fuel Cell, SOFC/GT - SOFC-GT combined system, SOFC/GT/ST - SOFC triple combined-cycle system.

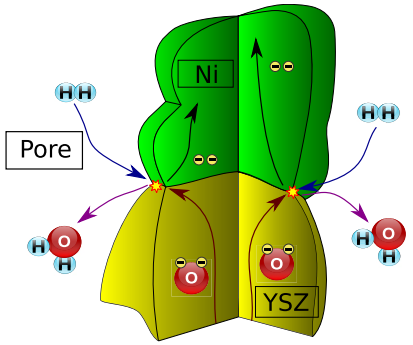

FIGURE 2. Schematical view on an electrochemical reaction in SOFC's anode with marked phases: YSZ is yttria-stabilized zirconia, Ni is nickel, Pore is empty space.

Scanning Electron Microscope (SEM) in a single system. A 3D reconstruction technique was introduced to the field of SOFCs by Wilson *et al.* [6] in 2006. The method enables the observation of many sequential 2D images of a porous microstructure and reconstructs it into three-dimensional digital models using advanced image processing. From the reconstructed microstructure, it is possible to quantify the microstructure parameters. These parameters are used to describe the relationships between the anode microstructure and the cell power generation. This is the procedure of the quantitative evaluation of the microstructure morphology. This opens a new perspective in SOFC studies: microstructure oriented modeling and design.

In a conventional approach, the microstructure optimization design is similar in its essence to the random search. Numerical simulations evaluate the performance of several electrodes with different microstructure morphologies. The best electrodes are fabricated and electrochemically tested. The feedback from the power generation experiment is then used to further modify the microstructure [7]–[9]. Using an optimization algorithm, this procedure can be significantly improved. Shi and Xue [10] conducted the first and so far the only attempt in the open literature (known to the authors) to use evolutionary algorithms for the optimization of an SOFC anode's microstructure. The authors combined a classical SOFC transport model and genetic algorithm (GA) to determine the optimal distributions of porosity and particle sizes for the electrodes [10]. This approach, although breaking new ground, has its limitations. The number of optimized parameters was restricted to porosity distribution and particle size. The impact of particles size on the reaction domain was estimated using a sphere packing algorithm, in which a contact angle was an adjustable parameter [10]. Moreover, the relations between the microstructural parameters were not included in the study [10]. The primary challenge to anode optimization still lies in the mathematical description of the relations between microstructural parameters. Collecting tomographic data binding a microstructure's parameters would take many years. Therefore, the generation of the synthetic microstructure is required to speed up the data collection. Shi and Xue [10] chose sphere packing to generate the synthetic microstructures, as it is the most common approach in the literature [11]. However, the random-packing algorithm was found to underestimate the tortuosity and triple phase boundary in comparison to the real microstructure [12]. The limitations of the sphere packing algorithm draw attention to the cellular automata (CA) simulations, which give a possibility of generating complex three-dimensional virtual structures. Cellular automata consist of many identical simple components, which together are capable of creating complex virtual structures. The cellular automata simulation was recently employed as a model of SOFC electrodes microstructure [13], [14]. Sebdani *et al.* [13] generated over 400 synthetic microstructures to find the one with the maximal reaction domain (TPB). The microstructures were generated randomly and therefore the algorithm falls into the category of random search. Furthermore, recent studies show that the performance of the cell can increase despite the decay of TPB [15]–[17]. Therefore, the more suitable optimization function should be built based on the output power.

C. AIM OF THIS WORK

The underlying motivation for this paper is to bridge the gap in the existing literature and provide a comprehensive optimization of SOFC anode microstructure. The research uses evolutionary algorithms and cellular automata simulation. The microstructural parameters obtained from the analysis of the synthetic microstructures are juxtaposed with FIB-SEM empirical data taken from the literature. We showed that the synthetic microstructures reflect the morphologies of the real electrode. The obtained results are used to solve the optimization problem. The optimization covers all the microstructural parameters and the relations between them. The optimization's objective function was built based on the maximum current density flowing through the cell under the chosen polarization. We have chosen GA for optimization, as a continuation of work done by Shi and Xue [10]. To increase the convergence of the optimization we have used a simpler and faster algorithm - particle swarm optimization (PSO) [18]. As the main objective of this paper is to provide

and prove the concept of the optimization we did not consider more complex algorithms.

This paper consists of the following parts: section II, a description of the physical model of SOFC, section III, the evaluation of the microstructural parameters correlations using the CA algorithm, section IV the introduction to the optimization algorithms used, section V, the verification of a physical model and the optimization algorithms, section VI, the results of the optimization and section VII, conclusions.

II. PHYSICAL MODEL OF SOFC ANODE

A. GOVERNING EQUATIONS

The transport phenomena to be considered are the diffusion of gases through the pore phase, the transport of electrons through an electron-conducting nickel phase and the transport of ions via an ion-conducting YSZ phase.

1) DIFFUSION OF GASEOUS SPECIES

The main fluxes contributing to mass transport in a porous electrode are a diffusive flux and a viscous flux. The viscous flow is driven by a pressure gradient and therefore is negligible compared to the diffusive flow in porous electrodes [19]. For the gaseous phase, the Fick's model has been chosen for its low computational complexity [20], [21]. It is based on the Bosanquet approximation of diffusivity and is expressed as follows:

$$\nabla \cdot \left(\frac{D_i^{\text{eff}}}{RT} \nabla P_i \right) = S_i, \tag{1}$$

where R is the gas constant, R = 8.314459848 J/(mol K), T is the temperature (K), D_i^{eff} is the effective diffusion coefficient (m^2/s), the subscript i denotes the chemical species: H_2 and H_2O. The mass source terms are due to the electrochemical reactions and they are calculated using Faraday law as follows:

$$s_{H_2} = \frac{i_{\text{TPB}}}{2\,F}, \quad s_{H_2O} = -\frac{i_{\text{TPB}}}{2F}, \tag{2}$$

where i_{TPB} is the volumetric exchange current density (A/m^3) and F is the Faraday constant, F = 96 485.3365 s A/mol. The formulation of i_{TPB} is described later, in Section II-B.

The effective diffusion coefficients in the porous anode are estimated by using the bulk diffusion coefficients of gases, the volume fraction and tortuosity factor of the pore phase:

$$D_i^{\text{eff}} = \frac{\varepsilon_{\text{pore}}}{\tau_{\text{pore}}} D_i. \tag{3}$$

The diffusion of the chemical components through the porous anode includes the Knudsen flow and the multicomponent diffusion. Therefore, the bulk diffusion coefficients used in Equation (3) come from the Maxwell-Stefan diffusion model [22] with the inclusion of the Knudsen diffusion term [23]:

$$D_i = \left(\frac{1}{D_{\text{K},i}} + \sum_{j \neq i} \frac{X_j}{D_{ij}} \right)^{-1}, \tag{4}$$

where $D_{\text{K},i}$ and D_{ij} are the Knudsen diffusion coefficient for component i and the binary diffusion coefficient for components i and j, respectively (m^2/s). The Knudsen diffusion coefficients $D_{\text{K},i}$ (m^2/s) are estimated by the following equation:

$$D_{\text{K},i} = \frac{d_{\text{p,pore}}}{2} \frac{2}{3} \sqrt{\frac{8RT}{\pi M_i}}, \tag{5}$$

where M_i is the molecular mass of component i (kg/mol), and $d_{\text{p,pore}}$ is the mean pore diameter (m). For the binary diffusion coefficients $D_{i,j}$ (m^2/s), the Fuller et al. method [24], [25] is adopted in this study:

$$D_{i,j} = \frac{14.3 T^{1.75} \sqrt{1/M_i + 1/M_j}}{\sqrt{2} P (\Sigma_i^{1/3} + \Sigma_j^{1/3})^2}, \tag{6}$$

where P is the pressure (atm.) and Σ_i is the diffusion volume of species i (1) obtained by summing the atomic diffusion volumes [24].

2) TRANSPORT OF THE ELECTRONS AND IONS

In the SOFC anodes, the electrons and oxide ions are transported through the Ni phase and the YSZ phase, respectively. Conservation equations for the electronic and ionic phase potentials are derived from the conservation of the charge and are expressed as follows:

$$\nabla \cdot \left(\sigma_{\text{ele}}^{\text{eff}} \nabla \phi_{\text{ele}} \right) = i_{\text{TPB}}, \tag{7}$$

$$\nabla \cdot \left(\sigma_{\text{ion}}^{\text{eff}} \nabla \phi_{\text{ion}} \right) = -i_{\text{TPB}}, \tag{8}$$

where ϕ_{ele} and ϕ_{ion} are the electric potential in the electron conductive phase (Ni) and the oxide-ion conductive phase (YSZ), respectively (V), and i_{TPB} is the volume-specific density of the current exchanged between the two phases (charge-transfer current) (A/m^3), $\sigma_{\text{ele}}^{\text{eff}}$ and $\sigma_{\text{ion}}^{\text{eff}}$ are the effective electronic and ionic conductivities (S/m), which are defined using the microstructural parameters and the bulk conductivities:

$$\sigma_{\text{ele}}^{\text{eff}} = \frac{\varepsilon_{\text{Ni}}}{\tau_{\text{Ni}}} \sigma_{\text{ele}}, \quad \sigma_{\text{ion}}^{\text{eff}} = \frac{\varepsilon_{\text{YSZ}}}{\tau_{\text{YSZ}}} \sigma_{\text{ion}}, \tag{9}$$

where ε_i and τ_i are the volume fraction and the tortuosity factor of the phase i, σ_{ele} and σ_{ion} are the conductivities of the bulk materials obtained from the literature [26], [27]:

$$\sigma_{\text{ele}} = 3.27 \cdot 10^6 - 1065.3\,T, \tag{10}$$

$$\sigma_{\text{ion}} = 3.4 \cdot 10^4 \exp\left(-\frac{10350}{T} \right), \tag{11}$$

where T is the temperature (K).

B. ELECTROCHEMICAL REACTION MODEL

The electrochemical reaction that occurs at the triple phase boundary of the SOFC anode is hydrogen molecule oxidation:

$$H_2 + O^{2-} \rightarrow H_2O + 2e^-. \tag{12}$$

One can proof that by applying the power law kinetic model to describe the backward and forward rates of the

reaction (12), the equation to calculate the exchange current density at TPB can be derived. The final form of the so-called Butler-Volmer equation varies depending on the application and in the case of SOFCs it has the following form [28]:

$$i_{\mathrm{TPB}} = i_0 \left[\exp\left(\frac{2\,F}{RT}\eta_{\mathrm{act}}\right) - \exp\left(-\frac{F}{RT}\eta_{\mathrm{act}}\right)\right], \quad (13)$$

where i_0 is the equilibrium exchange current density (A/m^3) and η_{act} is the activation overpotential (V).

The electric potential of the difference between the two solid phases are regarded as the sum of the activation overpotential η_{act} and the concentration overpotential η_{con}, and therefore the activation overpotential is derived as follows:

$$\eta_{\mathrm{act}} = \phi_{\mathrm{ele}} - \phi_{\mathrm{ion}} - \eta_{\mathrm{con}}, \quad (14)$$

where the electric potentials ϕ_{ele} and ϕ_{ion} are obtained by solving Equations (7) and (8) and the concentration overpotential is described by the following formula:

$$\eta_{\mathrm{conc}} = \frac{RT}{2\,F} \ln\left(\frac{P^{\mathrm{bulk}}_{\mathrm{H_2}}}{P_{\mathrm{H_2}}}\frac{P_{\mathrm{H_2O}}}{P^{\mathrm{bulk}}_{\mathrm{H_2O}}}\right), \quad (15)$$

where $P^{\mathrm{bulk}}_{\mathrm{H_2}}$ and $P^{\mathrm{bulk}}_{\mathrm{H_2O}}$ are the hydrogen and gaseous water partial pressure (Pa) at the anode surface and $P_{\mathrm{H_2}}$ and $P_{\mathrm{H_2O}}$ are the hydrogen and water vapor partial pressure (Pa) at the TPB region.

The equilibrium exchange current density i_0 (A/m^3) in the Butler-Volmer equation (Eq. (13)) depends on the microstructure of the anode and is a linear function of the TPB length density ℓ_{TPB} (m/m^3). It is written as follows:

$$i_0 = i_{0,\mathrm{TPB}}\ell_{\mathrm{TPB}}, \quad (16)$$

where $i_{0,\mathrm{TPB}}$ is the equilibrium exchange current per unit TPB length (A/m). In this study, the anode exchange current density is described by the following empirical equation obtained by fitting to the data obtained by de Boer [29]:

$$i_{0,\mathrm{TPB}} = 31.4\, P^{-0.03}_{\mathrm{H_2}} P^{0.4}_{\mathrm{H_2O}} \exp\left(\frac{-1.52\cdot 10^5}{RT}\right). \quad (17)$$

III. ESTIMATING AN ANODE'S MICROSTRUCTURE PARAMETERS CORRELATIONS

The anode's microstructure shows a great diversity of complex morphologies. Studying the origins of such complexity allows establishing the relation between microstructural parameters and consequently enables trustful microstructure optimization.

A. MICROSTRUCTURAL PARAMETERS

There are sixteen microstructural parameters describing an anode, connected with a grid of dependencies. For each of the three phases, the following parameters can be distinguished: 1) the phase volume fraction, describing the amount of a given phase, 2) connectivity, defining the fraction of the phase that contributes to the transport phenomena, 3) the tortuosity factor, which indicates the complexity of the phase and 4) the mean particle diameter and its standard deviation, which determine the grain size and how it differs from the average. An important parameter that directly affects the current density is a triple-phase boundary length density, which describes an amount of possible reaction domains.

B. MICROSTRUCTURE PARAMETERS EVALUATION

From the three-dimensional digital representation of microstructure, it is possible to estimate various microstructural parameters. For the quantification of the microstructural parameters, we employed the methodology developed by Iwai *et al.* [30], Vivet *et al.* [31], Kishimoto *et al.* [32], and Kishimoto [33]. Here, we present just a brief introduction to each of the used methods of quantification. For more details, please see the original papers [30]–[33].

The volume fraction of each phase was estimated based on voxel counts [30]. The algorithm checks the cross sections of the 3D reconstruction voxel by voxel and associates them with one of the three phases [30].

For the connectivity calculation, we have used the cluster neighborhood rule [31]. The voxels connected to the other voxels that represent the same phase form a cluster. Clusters are defined as percolated if they are connected to the boundary faces perpendicular to the x-axis. This is because of the directionality of the transport phenomena.

The average grain size was evaluated using a three-dimensional version of the intercept method applied to the digital representation of the microstructure [33]. In this method, a voxel is chosen [33]. Three lines along orthogonal coordinates are drawn in such way that they contain only voxels of the same phase [33]. The average length of these lines is a local particle size [33]. Average from all local particle sizes defines average grain size [33].

The tortuosity factor which directly describes the reduction rate of the diffusion coefficient in the porous media was estimated by the random walking procedure [32]. In this method, many walkers are stochastically distributed in the investigated phase. Each walker allots a neighbor voxel for the next movement [32]. From the rate of the reduction of the walkers' mean square displacement in the porous channels, compared to the displacement in the free space, the tortuosity factor is estimated [32].

The reaction sites (TPBs) were estimated using the volume expansion method [30] and Avizo software (Thermo Scientific$^{\mathrm{TM}}$Avizo$^{\mathrm{TM}}$). In this approach, each phase is virtually expanded. When all three phases overlap, the created volume contains the triple phase boundary that can be extracted by a centroid method [30].

1) GENERATING SYNTHETIC MICROSTRUCTURES

Mathematical models called cellular automata can artificially generate the variety of complex microstructures [13], [14]. By analyzing microstructures, one may establish the relationships between the microstructural parameters for the considered electrode.

In the presented approach, an empty cuboid of wanted geometrical dimension is formed, the obtained volume is

interpreted as a pore phase. In this volume, the cellular automata start from generating two types of seeds that after growing will constitute the nickel and yttria-stabilized zirconia phases. The seeds generation is subjected to the local rules that prevent generating one phase being encompassed by the other which are rather unlikely to occur in the real anode. These rules are based on the geometrical relations between seeds. Every time a new seed is generated, a position in space in which it can be put is searched and analyzed. If there are too many seeds of the same phase or any seed of a different phase that are too close to the candidate position for a seed, this position is not accepted. The number of possible neighboring seeds with similar space is arbitrary. The area around the candidate space position is searched two times with a different volume and rules. The analyzed space is defined by a fraction of the grow radius of the generated seed's phase in the first search and by a fraction of the biggest grow radius of all phases in the second search. The second search detects only seeds representing a different phase than considered in the iteration. Fractions of the grow radius are chosen arbitrarily. The order of the seed drawing impact on the final microstructure shape should be analyzed. We generated the Ni seeds before the YSZ seeds, as the Ni phase seeds have a higher tendency to agglomerate. In the next step, the states of the voxel neighboring seeds are updated according to a deterministic function to create a sphere-like shape. For each seed, the grow radius is determined from the Gauss normal distribution with the mean and standard deviation values being the input parameters. The number of seeds is a function of the desired average grain size and the volume of the generated microstructure and is adjusted iteratively repeating initial generation and growth with a different number of seeds. The procedure is continued until the volume fraction discrepancies of around 4% from the desired are obtained.

As a next step, the new generation of seeds is distributed in each phase. Each phase can host only seeds of the same phase. One seed is generated in a given distance from the phase surface. The seed is growing until the created radius violates the space of the competitive phase or its radius becomes greater than the arbitrary maximum value. The new voxels are adopted and the growth stops. Because each seed disturbs the existing volume only by a few voxels, a large number of around 300 000 (200 000 - 500 000) seeds is required to mimic the natural microstructure for the resolution of 280x280x280 voxels. The grow radius and its standard deviation of seeds were calibrated by the comparison with the real microstructures observed using FIB-SEM electron tomography. At this stage, the obtained microstructure can reproduce the desired volume fraction with the precision of a few voxels difference per million voxels. The comparison between the cross sections of a real SOFC's anode microstructure from the FIB-SEM observation after the ternarization of original SEM image and a picture of a synthetically generated microstructure is presented in Fig. 3.

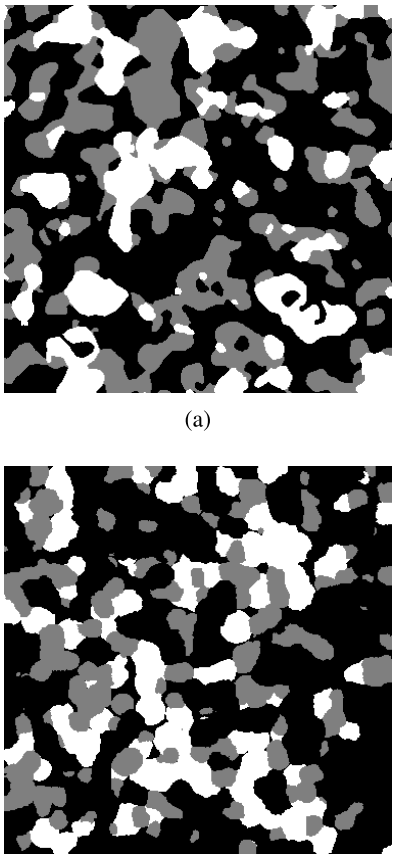

FIGURE 3. An example of the segmented microstructure cross sections, a) real microstructure obtained by FIB-SEM electron tomography and b) synthetic microstructure generated by CA algorithm. White is Ni, gray is YSZ and black is pore.

The typical characteristics of an anode's microstructure are preserved - the nickel phase is agglomerated more than the YSZ phase, the solid phases are in contact with each other. The microstructure generation algorithm is represented in a flowchart in Fig. 4. An example of different three-dimensional digital representations of synthetically generated microstructures is presented in Fig. 5.

2) RESULTS FROM SYNTHETIC MICROSTRUCTURES ANALYSIS

To investigate the relationship between microstructural parameters we generated numerous three-dimensional synthetic microstructures with a size of 10 μm × 10 μm × 10 μm, which are typical dimensions of FIB-SEM samples [34]. All of the obtained digital representations of the microstructures were quantitatively analyzed using the methodology described in section III-B. An example of the obtained 3D reconstructions is presented in Fig. 5. As can be seen, we could successfully cover a wide range of anode compositions from low to high content of nickel, pores and YSZ. When the microstructure is homogeneous and particle size does not differ significantly, the reaction domain can be treated as a function of particle diameter [35], [36].

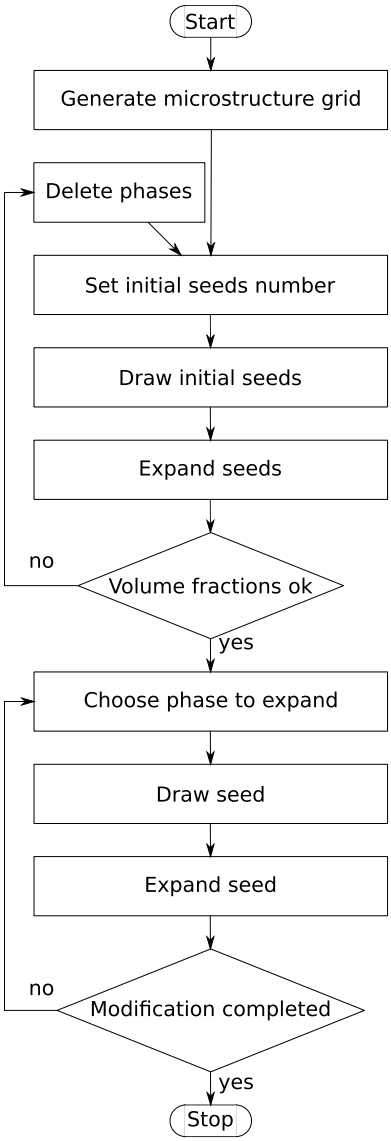

FIGURE 4. Flowchart for the microstructure generation algorithm.

The triple-phase boundary length density for highly percolated anode versus the maximum mean particle diameter dependency is presented in Fig. 6. The maximum mean particle diameter is the biggest particle size from Ni, YSZ or pore. The results include the estimation based on the synthetic microstructures as well as the data taken from the literature (Fig. 6).

Figure 7 shows a loss of reaction domain in the case when one phase loses its percolation. By defining the reaction domain as $\ell_{\mathrm{TPB}} = \hat{\ell}_{\mathrm{TPB}}\zeta_{\mathrm{Ni}}\zeta_{\mathrm{YSZ}}\zeta_{\mathrm{pore}}$, we assure that the connectivity loss of all phases is included. Figure 8 contains information about the dependence between connectivity and the volume fraction obtained by several synthetic microstructures analysis. The connectivity threshold seems to be exactly at the volume fraction of 20%. In comparison to the data taken from the literature [39] marked as red squares at Fig. 8, the connectivity values from the synthetic microstructures are in good agreement with the experiment.

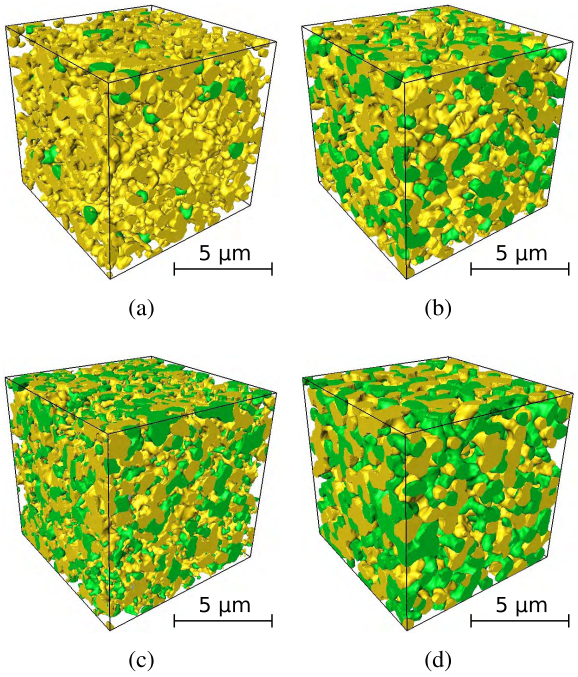

FIGURE 5. Examples of synthetic microstructures generated in this study. Yellow is YSZ, green is nickel and void represents pores. a) 5% Ni, 40% YSZ, Particle diameters: $d_{\mathrm{p,Ni}} = 0.63$ μm, $d_{\mathrm{p,YSZ}} = 0.78$ μm, $d_{\mathrm{p,pore}} = 1.3$ μm, b) 20% Ni, 40% YSZ, Particle diameters: $d_{\mathrm{p,Ni}} = 0.73$ μm, $d_{\mathrm{p,YSZ}} = 0.87$ μm, $d_{\mathrm{p,pore}} = 1.04$, μm c) 25% Ni, 40% YSZ, Particle diameters: $d_{\mathrm{p,Ni}} = 0.46$ μm, $d_{\mathrm{p,YSZ}} = 0.55$ μm, $d_{\mathrm{p,pore}} = 0.62$ μm, d) 33% Ni, 33% YSZ, Particle diameters: $d_{\mathrm{p,Ni}} = 0.95$ μm, $d_{\mathrm{p,YSZ}} = 0.97$ μm, $d_{\mathrm{p,pore}} = 1.04$ μm.

The tortuosity factors of all phases were estimated using the approximation to the experimental data from [33] and the data from the synthetic microstructures. The results of the fitting are presented in Fig. 9. As can be seen in the figure, the tortuosity factors obtained for the synthetic microstructures follow the trend established by the experimental data. This observation holds for all investigated phases. The approximation equations take the following form:

$$\tau_{\mathrm{Ni}} = 681.70e^{-13.025\varepsilon_{\mathrm{Ni}}} + 1, \tag{18}$$

$$\tau_{\mathrm{YSZ}} = 171.76e^{-9.9202\varepsilon_{\mathrm{YSZ}}} + 1, \tag{19}$$

$$\tau_{\mathrm{pore}} = 37.119e^{-7.5246\varepsilon_{\mathrm{pore}}} + 1. \tag{20}$$

IV. EVOLUTIONARY ALGORITHMS

The three primary parts of every optimization algorithm decide if it falls into the category of evolutionary computing. The first part is the process of initialization where the initial population of individuals is randomly generated according to a solution representation. Each individual within the population represents a possible solution to the considered optimization problem. During the second part, all individuals in the population are evaluated using the so-called fitness function. The obtained fitness values determine the direction of the population evolution. The third process is the generation of a new population by the interactions of solutions in the existing population. In the presented work two basic evolutionary algorithms have been used: genetic algorithm (GA) and

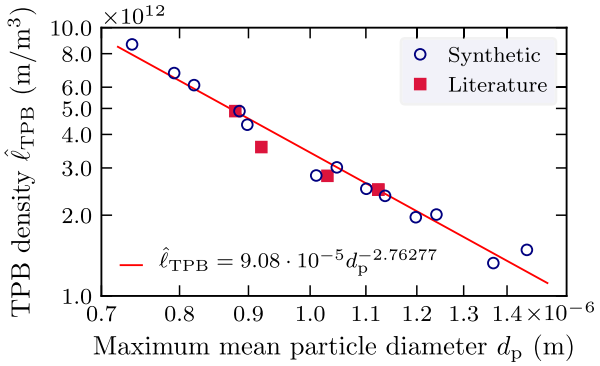

FIGURE 6. The available reaction sites ($\hat{\ell}_{\mathrm{TPB}}$) for a highly percolated anode as a function of a mean particle diameter (d_{p}). The blue circles are the values obtained from the quantitative analysis of the synthetic microstructures, and the red squares represent the real TPB densities obtained from the experiments [15]–[17], [37], [38].

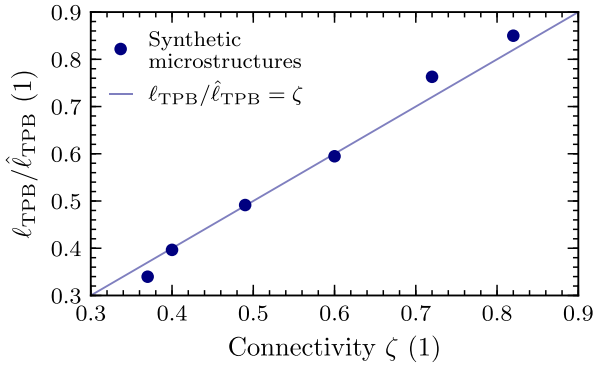

FIGURE 7. The decay of the electrochemical reaction domain as a function of connectivity of least percolated phase with full percolation of two other phases.

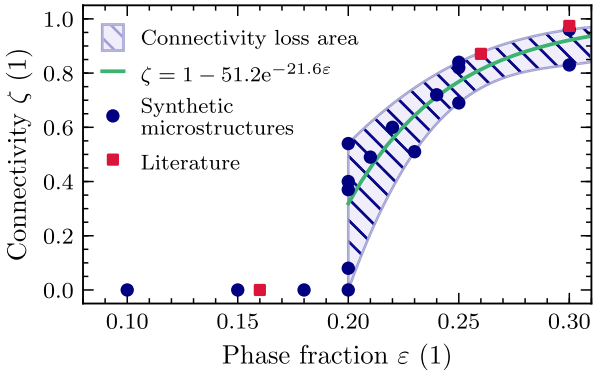

FIGURE 8. Phase connectivity as a function of phase fraction. Literature data from [39].

particle swarm optimization (PSO). Both are shortly addressed here [40].

A. PROBLEM REPRESENTATION AND FITNESS FUNCTION

Every anode was assumed to be described by three independent microstructural parameters: the volume fraction of Ni, the volume fraction of YSZ and the average pore diameter. The phase volume fraction was selected in the range

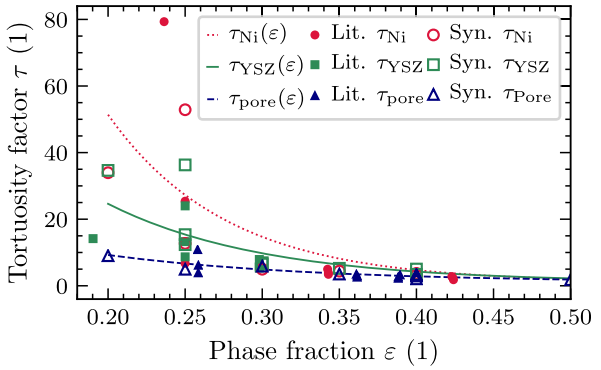

FIGURE 9. The tortuosity factor as a function of the phase fraction. Experimental data from [33].

from 0.2 to 0.6 and the average particle size in the range from 1 μm to 3 μm. These parameters were randomly chosen for the first generation of solutions. Other microstructural parameters such as the tortuosity factors, the connectivities of the phases and the triple phase boundary length densities were treated as dependent variables and they were calculated afterward, using the relations derived from the analysis of the synthetic microstructures, presented in Section III.

Additional parameters and system conditions were fixed. The fixed parameters are: the thickness of an anode which has a value of 50 μm, the system temperatures, of which we performed optimization, were 800 °C, 900 °C and 1000 °C, the system pressure with a value of 101300 Pa, the total overpotential with a value of 0.05 V and the inlet gas composition - 97% H_2, 3% H_2O. These parameters were chosen to mimic the real SOFC operating conditions. The parameters mentioned above were employed in the mathematical model described in Section II. The model was used to calculate the distribution of volume-specific exchange current density (see Eq. (13)). Then, the distribution of i_{TPB} is utilized to compute the fitness function as it is presented below:

$$j = \int_0^{L_{\mathrm{a}}} i_{\mathrm{TPB}} \mathrm{d}x, \tag{21}$$

where L_{a} is an anode thickness. Therefore, the returned value j of the fitness function is the current density generated by the anode (A/cm^2), which needs to be maximized.

B. GENETIC ALGORITHM

A genetic algorithm can be summarized as follows: firstly, the population of chromosomes is randomly generated [41], [42]. Each chromosome represents a set of microstructural parameters which represents a possible microstructure of a SOFC anode [41]. These parameters are the volume fraction of Ni and YSZ and the particle size of pores. A chromosome is generated as a string of binary values, that can be mapped onto a physical range of values with precision dependent from the chromosome length [41], [42]. A multiple number of variables can be represented as one chromosome. Each variable is assigned to a fragment of the chromosome [42]. For part of the chromosome of the length l representing a

variable x, this string can be treated as an integral number in the range from 0 to 2^l in binary form that is mapped linearly to a specified interval $[x_{\min}, x_{\max}]$ [42].

In the case of anode encoding precisions were 10^{-9} for the volume fraction and $10^{-6}\mu$m for the particle size. Then, all individuals are evaluated using the fitness function, described by Eq. (21), which requires the solution of the mathematical model, described in Section II.

The evaluation procedure assesses the relationship between the microstructure and produced current. Individuals with good fitness have a higher possibility to pass their chromosomes to the offspring generation [41], [42]. Based on the fitness function, the parent chromosomes are selected [41], [42]. The selection was performed using the stochastic remainder selection without replacement [42]. In this method the expected number of each individual in parents pool is estimated as an individual's fitness divided by a mean fitness of the current population and multiplied by the parents pool population size:

$$\mathrm{E}(k) = \frac{j_k}{\sum_k j_k}\bar{N}, \tag{22}$$

where k is the id number of an individual, $\mathrm{E}(k)$ is the expected number of k individual in the parents pool, j_k is the fitness of k individual according to Eq. 21 and $\bar{N}$ is the parents pool population size. A number of copies equal to the integer part of $\mathrm{E}(k)$ of individual k is put into the parents pool. After this step, the draw takes place until all the parents are selected. One by one, individuals have a chance equal to the fractional part of the expected number $\mathrm{E}(k)$ to get a copy in parents pool [42]. After this step, the parents are matched randomly. The crossover and mutation operators make the offspring population [41], [42]. As a crossover operator, we used a one-point crossover. In this basic crossover two offspring arise from the two parents. The random point of the crossover is selected, then the first child has its chromosome made up from the first part of the first parent and the second part from the second parent. The second child takes the first part from the second parent and the second part from the first parent. Mutation - sporadic small modification of a chromosome - is performed with the constant probability of one percent for each gene in the chromosome during the whole optimization process [41], [42]. The new population is created from the new offspring population and two best individuals from the old population (elitism) [41], [42]. These operations lead towards the optimal solution, which is obtained after several generations [41], [42]. As a result, the anode with the microstructure, which leads to a high current production, is obtained. The block scheme of the GA algorithm is shown in Fig. 10.

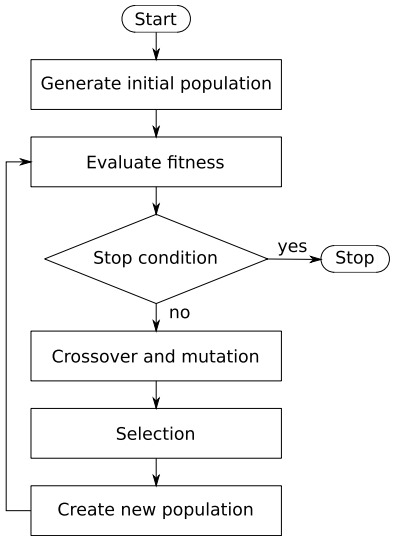

FIGURE 10. Flowchart for the genetic algorithm.

C. PARTICLE SWARM OPTIMIZATION

The particle swarm optimization is an algorithm that optimizes a problem iteratively in a similar fashion as the genetic algorithm [40]. PSO improves a candidate solution concerning a given measure of quality. Here, the measure of quality is the amount of the current generated by the anode, evaluated by the mathematical model (see Section II) and previously proposed fitness function (see Eq. 21).

The PSO method optimizes the problem with a random population of candidate solutions, which are represented by particles. Each particle is a set of microstructural parameters, which represents the potential anode of an SOFC. These parameters are the same as in GA - the Ni and YSZ volume fractions and mean pore particle diameter in the same range of possible values. Unlike the GA, the PSO operates on the real representation of the optimized parameters. These particles are moved in the search space according to the particle's actual position and velocity [43]. The position represents a vector of the optimized microstructure parameters. The velocity is a direction of change of these parameters [43]. Each particle's movement is influenced by its best-known location as well as by the position of the particle with the best fitness in the population, which move the swarm towards the best solutions [43]. Every particle k in the population is characterized by its position $\boldsymbol{X}_k$, the best previous position $\boldsymbol{P}_k$, velocity $\boldsymbol{V}_k$ and fitness, which is the value returned by the fitness function [43], given here by Eq. 21. The particle position in the next generation is computed using the following formula [43]:

$$\boldsymbol{X}_k^{n+1} = \boldsymbol{X}_k^n + \boldsymbol{V}_k^n, \tag{23}$$

where n is the generation number.

Particle velocity is computed in every generation and is given by [44]:

$$\boldsymbol{V}_k^{n+1} = \omega \boldsymbol{V}_k^n + \mathrm{c}_1 \mathrm{rand}\,() \left(\boldsymbol{P}_k - \boldsymbol{X}_k^n\right) + \mathrm{c}_2 \mathrm{rand}\,() \left(\boldsymbol{P}_g^n - \boldsymbol{X}_k^n\right). \tag{24}$$

The value of inertia weight ω is proposed in [44] as a function of time. $\boldsymbol{P}_g$ is the position of the best particle from a whole population in the current generation [43], rand is a function,

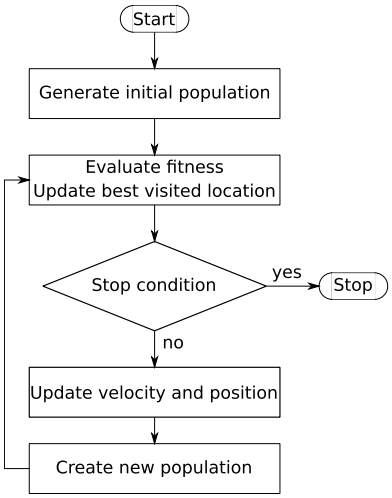

FIGURE 11. Flowchart for particle swarm optimization algorithm.

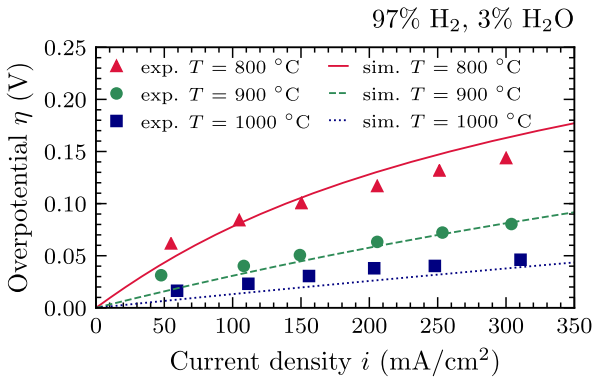

FIGURE 12. Overpotential calculated by the fitness function versus the experimental data [37].

which generates random numbers in the range [0, 1) [43]. Constants c_1 and c_2 are equal to 2 [43]. The inertia weight ω is changing linearly with time according to the given formula:

$$\omega(n) = 0.4 + 0.8\frac{N-n}{N}, \tag{25}$$

where N is a maximum possible number of generations. The block scheme of the PSO algorithm is shown in Fig. 11.

V. VERIFICATION OF THE ALGORITHMS

A. VERIFICATION OF THE FITNESS FUNCTION

Before conducting an optimization process, the fitness function was verified using the empirical data from the open literature [37]. Figure 12 presents the experimental data from [37] versus the computation from the present studies. The results shown in Fig. 12 represents the anode overpotential as a function of the current density. The results of the simulation are in good agreement with the empirical data taken from the literature [37]. It can be concluded that the fitness function can successfully predict anode polarization and therefore it can be applied to the optimization process.

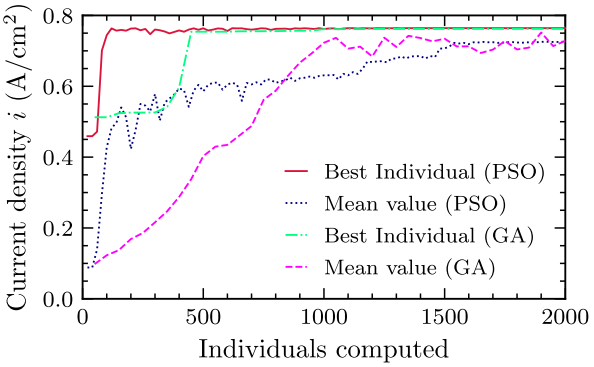

FIGURE 13. The improvement of the anode microstructure through the PSO and GA algorithms progress for the operating temperature 1000 °C.

B. VERIFICATION OF THE EVOLUTIONARY ALGORITHMS

For the performance evaluation, the Rastrigin and Shaffer functions have been used for their multimodal and deceptive character [45], [46]. Both functions are the primary benchmarking functions used for the testing of evolutionary algorithms [45], [46]. Tests of both algorithms ensured that the algorithms were correctly implemented and can be used for complex optimizations. Furthermore, the conducted tests provided information on how to set and correct parameters using data from a population evolution.

VI. ANODE MICROSTRUCTURE OPTIMIZATION RESULTS

After successful verification of the fitness function and the evolutionary algorithms, we conducted the optimization of the solid oxide fuel cell anode's microstructure parameters. The microstructural parameters are related by the network of dependencies typical for a conventional anode. As a consequence, we look after only for those settings that can be decided independently during the manufacturing process. Those parameters are the anode composition and particle size. The rest of the parameters are estimated afterward from the correlations collected from the literature and the analysis of the synthetic microstructures (see Section III for details). It is worth to mention that during optimization we do not differentiate between the particle size of different phases. Here we assume homogeneous and uniform particle size distribution for all phases. This is because the phase with the biggest particle size will have the highest impact on the maximum possible reaction domain (ℓ_{TPB}). The optimization process was performed until one of the converge criteria was met. As a stop conditions, we have used the maximum number of iterations and lack of the improvement of the best solution for ten generations. The maximum number of iterations was selected to ensure that the average value of the fitness function in the last generation was close to the best solution. The temperature range of the optimization was chosen from 800 °C to 1000 °C, as it is conventional SOFC operating a range of temperatures. Additionally, the verification of the physical model was performed in this temperature range.

TABLE 1. The best microstructure parameters obtained using the GA and PSO.

Operating conditions			
Parameter	**Condition A**	**Condition B**	**Condition C**
T	800 °C	900 °C	1000 °C
Optimized microstructural parameters			
Parameter	**Condition A**	**Condition B**	**Condition C**
$\varepsilon_{\mathrm{Ni}}$	0.246	0.240	0.234
$\varepsilon_{\mathrm{YSZ}}$	0.502	0.501	0.488
d_p	$1{\cdot}10^{-6}$ m	$1{\cdot}10^{-6}$ m	$1{\cdot}10^{-6}$ m
Dependent microstructural parameters			
Parameter	**Condition A**	**Condition B**	**Condition C**
$\varepsilon_{\mathrm{Pore}}$	0.252	0.259	0.278
τ_{Ni}	28.67	30.69	33.15
τ_{YSZ}	2.18	2.20	2.36
τ_{pore}	6.57	6.29	5.60
ζ_{Ni}	0.748	0.717	0.677
ζ_{YSZ}	0.999	0.999	0.999
ζ_{pore}	0.778	0.809	0.873
ℓ_{TPB}	$1.99{\cdot}10^{12}$ m/m^3	$1.98{\cdot}10^{12}$ m/m^3	$2.01{\cdot}10^{12}$ m/m^3
Anode's performance			
Parameter	**Condition A**	**Condition B**	**Condition C**
i	0.144 A/cm^2	0.380 A/cm^2	0.764 A/cm^2

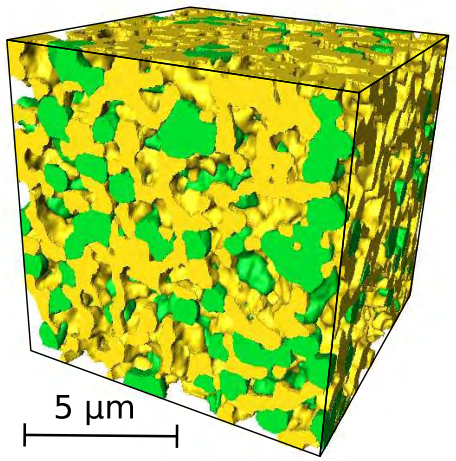

FIGURE 14. Visualization of the optimal synthetic microstructure described by the parameters obtained by the evolutionary algorithms.

The objective is to find the anode microstructure composition, for which the maximum current value can be obtained. The example of the best anode performance and a mean value through the PSO and GA algorithms progress is shown in Fig. 13. The figure indicates that even though both algorithms lead to the same anode composition, the PSO algorithm converges to the global optimum five times faster than the genetic algorithm in the investigated case.

The summary of the obtained results are presented in Table 1. The results suggest the lowest possible values

TABLE 2. Optimal microstructure.

Operating conditions			
Parameter	**Value**		
T	800–1000 °C		
Microstructural parameters			
Parameter	**Optimized**	**Conventional** [37]	**Unit**
$\varepsilon_{\mathrm{Ni}}$	0.25	0.253	1
$\varepsilon_{\mathrm{YSZ}}$	0.5	0.251	1
$\varepsilon_{\mathrm{pore}}$	0.25	0.496	1
$d_{\mathrm{p,Ni}}$	$0.79{\cdot}10^{-6}$	$1.12{\cdot}10^{-6}$	m
$d_{\mathrm{p,YSZ}}$	$0.95{\cdot}10^{-6}$	$0.53{\cdot}10^{-6}$	m
$d_{\mathrm{p,pore}}$	$0.72{\cdot}10^{-6}$	$0.97{\cdot}10^{-6}$	m
τ_{Ni}	16.21	6.91	1
τ_{YSZ}	2.48	8.85	1
τ_{pore}	5.29	1.74	1
ζ_{Ni}	0.877	0.842	1
ζ_{YSZ}	0.999	0.943	1
ζ_{pore}	0.997	1.00	1
ℓ_{TPB}	$3.7{\cdot}10^{12}$	$2.49\cdot10^{12}$	m/m^3
Anode's performance			
Parameter	**Optimized**	**Conventional**	**Unit**
i	0.182–0.886	0.059–0.402	A/cm^2

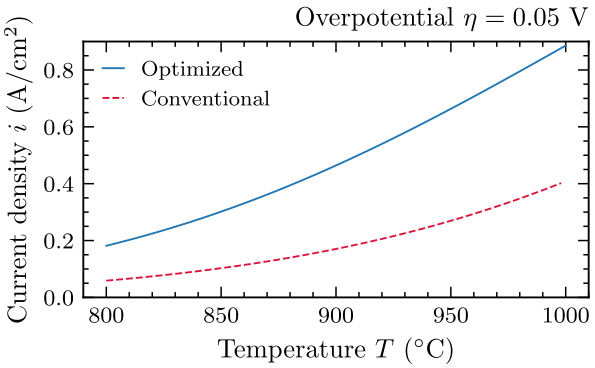

FIGURE 15. SOFC current density versus the operating temperature for the optimized and conventional anodes operating with overpotential of 0.05 V.

of the particle diameter. The algorithm minimizes the nickel content until the phase is sufficiently percolated.

The optimal fractions of Ni, YSZ and the pores obtained from the evolutionary algorithms have been rounded to take into account the possibilities of the anode manufacturing process. This microstructure was then digitally generated and analyzed using the methods described in Section III-B. The visualization of the optimal synthetic microstructure is shown in Fig. 14 and the parameters are juxtaposed in Table 2.

The comparison between the conventional anode (data from [37]) and the optimized anodes are presented in the form of the relation between the overpotential and current density in Fig. 15 and in the form of the polarization curves in Fig. 16. The optimized microstructure provides twice as much current

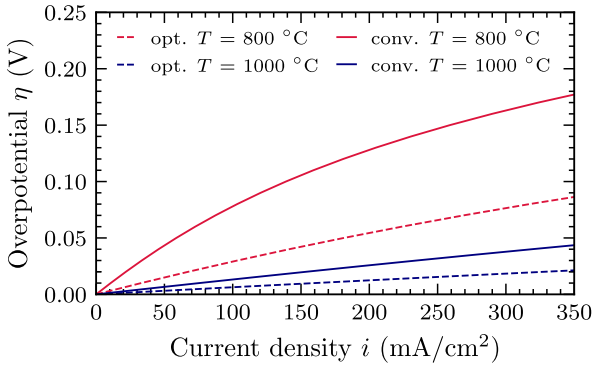

FIGURE 16. Polarization curves of the conventional and optimal anodes.

density in all the investigated range of potential operating conditions.

VII. CONCLUSION

In this paper, we presented a new approach to the optimization of a solid oxide fuel cell anode's microstructure. The optimization was conducted by the combination of numerical modeling of transport phenomena, cellular automata, and the evolutionary algorithms. The biggest challenge lied in the unknown relations between microstructural parameters that are crucial for reliable optimization. The complex description of such a problem was not available in the literature due to the extensive time needed for the quantitative analysis of microstructures' tomographic data. We addressed this issue by the quantitative study of the 3D digital representations of microstructures generated by the cellular automata simulation. Those synthetic microstructures were proved to be a valid representation of a real microstructure by a number of comparisons to empirical data which was obtained from the FIB-SEM electron tomography. The presented algorithm for generating synthetic microstructures can be used as a basis for applications in various fields of materials science.

Moreover, the genetic algorithm, which was conventionally used before in the field of SOFC optimization was replaced by much faster particle swarm optimization. This approach opens the possibility for the optimization of more complex electrodes or the entire cells in the future.

Presumably, the presented optimization results favor the volume fraction of the ion conductor as the ion diffusion is the slowest process. The volume fractions of pores and nickel, responsible for gas diffusion and electron flow respectively, follow the trend. The simulation gives the quantitative value of the optimal anode's composition and shows microstructure dependency on temperature and fuel composition which allows tailoring the microstructure for the particular application. Most importantly, the presented methodology can be extended to unconventional anodes, where the set of optimized parameters can be larger.

REFERENCES

[1] O. Z. Sharaf and M. F. Orhan, "An overview of fuel cell technology: Fundamentals and applications," *Renew. Sustain. Energy Rev.*, vol. 32, pp. 810–853, Apr. 2014.

[2] A. Kirubakaran, S. Jain, and R. K. Nema, "A review on fuel cell technologies and power electronic interface," *Renew. Sustain. Energy Rev.*, vol. 13, no. 9, pp. 2430–2440, 2009.

[3] S. Srinivasan, *Fuel Cells: From Fundamentals to Applications*. New York, NY, USA: Springer, 2006.

[4] J. Larmine and A. Dicks, *Fuel Cell Systems Explained*. Chichester, U.K.: Wiley, 2003.

[5] Y. Kobayashi, Y. Ando, T. Kabata, M. Nishiura, K. Tomida, and N. Matake, "Extremely high-efficiency thermal power system-solid oxide fuel cell (SOFC) triple combined-cycle system," *Mitsubishi Heavy Ind. Tech. Rev.*, vol. 48, no. 3, pp. 9–15, Sep. 2011.

[6] J. R. Wilson *et al.*, "Three-dimensional reconstruction of a solid-oxide fuel-cell anode," *Nature Mater.*, vol. 5, Jun. 2006, Art. no. 541.

[7] S. P. Jiang and S. H. Chan, "A review of anode materials development in solid oxide fuel cells," *J. Mater. Sci.*, vol. 39, no. 14, pp. 4405–4439, Jul. 2004.

[8] M. Kishimoto, M. Lomberg, E. Ruiz-Trejo, and N. P. Brandon, "Enhanced triple-phase boundary density in infiltrated electrodes for solid oxide fuel cells demonstrated by high-resolution tomography," *J. Power Sources*, vol. 266, pp. 291–295, Nov. 2014.

[9] Z. Han, Z. Yang, and M. Han, "Optimization of Ni-YSZ anodes for tubular SOFC by a novel and efficient phase inversion-impregnation approach," *J. Alloys Compounds*, vol. 750, pp. 130–138, Jun. 2018.

[10] J. Shi and X. Xue, "Optimization design of electrodes for anode-supported solid oxide fuel cells via genetic algorithm," *J. Electrochem. Soc.*, vol. 158, no. 2, pp. B143–B151, 2011.

[11] Q. Cai, C. S. Adjiman, and N. P. Brandon, "Modelling the 3D microstructure and performance of solid oxide fuel cell electrodes: Computational parameters," *Electrochim. Acta*, vol. 56, no. 16, pp. 5804–5814, 2011.

[12] Y. Zhang, Y. Wang, Y. Wang, F. Chen, and C. Xia, "Random-packing model for solid oxide fuel cell electrodes with particle size distributions," *J. Power Sources*, vol. 196, no. 4, pp. 1983–1991, Feb. 2011.

[13] M. M. Sebdani, M. Baniassadi, J. Jamali, M. Ahadiparast, K. Abrinia, and M. Safdari, "Designing an optimal 3D microstructure for three-phase solid oxide fuel cell anodes with maximal active triple phase boundary length (TPBL)," *Int. J. Hydrogen Energy*, vol. 40, no. 45, pp. 15585–15596, 2015.

[14] J. Joos, "Modelling and simulation of mixed ionic/electronic conducting (MIEC) cathodes," in *Microstructural Characterisation, Modelling and Simulation of Solid Oxide Fuel Cell Cathodes*. Karlsruhe, Germany: KIT Scientific, 2017, ch. 5, sec. 7, pp. 149–150.

[15] G. Brus *et al.*, "Local evolution of three-dimensional microstructure morphology of planar anode-supported SOFC," *ECS Trans.*, vol. 68, no. 1, pp. 1237–1244, Jul. 2015.

[16] G. Brus, H. Iwai, Y. Otani, M. Saito, H. Yoshida, and J. S. Szmyd, "Local evolution of triple phase boundary in solid oxide fuel cell stack after long-term operation," *Fuel Cells*, vol. 15, no. 3, pp. 545–548, Jun. 2015.

[17] G. Brus, H. Iwai, A. Sciazko, M. Saito, H. Yoshida, and J. S. Szmyd, "Local evolution of anode microstructure morphology in a solid oxide fuel cell after long-term stack operation," *J. Power Sources*, vol. 288, pp. 199–205, Aug. 2015.

[18] R. Hassan, B. Cohanim, O. de Weck, and G. Venter, "A comparison of particle swarm optimization and the genetic algorithm," in *Proc. 46th AIAA/ASME/ASCE/AHS/ASC Struct., Struct. Dyn. Mater. Conf.*, Austin, TX, USA, Apr. 2005, p. 1897.

[19] Y. Jiang and A. V. Virkar, "Fuel composition and diluent effect on gas transport and performance of anode-supported SOFCs," *J. Electrochem. Soc.*, vol. 150, no. 7, pp. A942–A951, 2003.

[20] Y. Fu *et al.*, "Multicomponent gas diffusion in porous electrodes," *J. Electrochem. Soc.*, vol. 162, no. 6, pp. F613–F621, 2015.

[21] R. Suwanwarangkul, E. Croiset, M. W. Fowler, P. L. Douglas, E. Entchev, and M. A. Douglas, "Performance comparison of Fick's, dusty-gas and Stefan–Maxwell models to predict the concentration overpotential of a SOFC anode," *J. Power Sources*, vol. 122, no. 1, pp. 9–18, Jul. 2003.

[22] G. Brus, "Experimental and numerical studies on chemically reacting gas flow in the porous structure of a solid oxide fuel cells internal fuel reformer," *Int. J. Hydrogen Energy*, vol. 37, no. 22, pp. 17225–17234, Nov. 2012.

[23] W. Lehnert, J. Meusinger, and F. Thom, "Modelling of gas transport phenomena in SOFC anodes," *J. Power Sources*, vol. 87, nos. 1–2, pp. 57–63, Apr. 2000.

[24] E. N. Fuller, K. Ensley, and J. C. Giddings, "Diffusion of halogenated hydrocarbons in helium. The effect of structure on collision cross sections," *J. Phys. Chem.*, vol. 73, no. 11, pp. 3679–3685, Nov. 1969.

[25] B. E. Poling, J. M. Prausnitz, and J. P. O'Connell, "Diffusion coefficients for binary gas systems at low pressures: Empirical correlations," in *The Properties of Gases and Liquids*, 5th ed. New York, NY, USA: McGraw-Hill, 2001, ch. 11, sec. 4, p. 11.10.
[26] U. Anselmi-Tamburini, G. Chiodelli, M. Arimondi, F. Maglia, G. Spinolo, and Z. A. Munir, "Electrical properties of Ni/YSZ cermets obtained through combustion synthesis," *Solid State Ionics*, vol. 110, nos. 1–2, pp. 35–43, Jul. 1998.
[27] N. F. Bessette, II, W. J. Wepfer, and J. Winnick, "A mathematical model of a solid oxide fuel cell," *J. Electrochem. Soc.*, vol. 142, no. 11, pp. 3792–3800, 1995.
[28] T. Kawada, N. Sakai, H. Yokokawa, M. Dokiya, M. Mori, and T. Iwata, "Characteristics of slurry-coated nickel zirconia cermet anodes for solid oxide fuel cells," *J. Electrochem. Soc.*, vol. 137, no. 10, pp. 3042–3047, 1990.
[29] B. de Boer, "SOFC anode. Hydrogen oxidation at porous nickel and nickel/zirconia electrodes," Ph.D. dissertation, Univ. Twente, Enschede, The Netherlands, 1998.
[30] H. Iwai *et al.*, "Quantification of SOFC anode microstructure based on dual beam FIB-SEM technique," *J. Power Sources*, vol. 195, no. 4, pp. 955–961, Feb. 2010.
[31] N. Vivet *et al.*, "3D microstructural characterization of a solid oxide fuel cell anode reconstructed by focused ion beam tomography," *J. Power Sources*, vol. 196, no. 18, pp. 7541–7549, Sep. 2011.
[32] M. Kishimoto, H. Iwai, M. Saito, and H. Yoshida, "Quantitative evaluation of transport properties of SOFC porous anode by random walk process," *ECS Trans.*, vol. 25, no. 2, pp. 1887–1896, 2009.
[33] M. Kishimoto, "Three-dimensional microstructure of solid oxide fuel cell anode: Observation, quantification, and application to numerical analysis," Ph.D. dissertation, Kyoto Univ., Kyoto, Japan, 2013.
[34] W. K. Epting *et al.*, "Quantifying intermediate-frequency heterogeneities of SOFC electrodes using X-ray computed tomography," *J. Amer. Ceram. Soc.*, vol. 100, no. 5, pp. 2232–2242, May 2017.
[35] W. Zhu, D. Ding, and C. Xia, "Enhancement in three-phase boundary of SOFC electrodes by an ion impregnation method: A modeling comparison," *Electrochem. Solid-State Lett.*, vol. 11, no. 6, pp. B86–B93, 2008.
[36] X. Lu *et al.*, "Correlation between triple phase boundary and the microstructure of solid oxide fuel cell anodes: The role of composition, porosity and Ni densification," *J. Power Sources*, vol. 365, pp. 210–219, Oct. 2017.
[37] M. Kishimoto, H. Iwai, M. Saito, and H. Yoshida, "Quantitative evaluation of solid oxide fuel cell porous anode microstructure based on focused ion beam and scanning electron microscope technique and prediction of anode overpotentials," *J. Power Sources*, vol. 196, no. 10, pp. 4555–4563, May 2011.
[38] G. Brus, H. Iwai, Y. Otani, M. Saito, H. Yoshida, and J. S. Szmyd, "Local evolution of three-dimensional microstructure of Ni-YSZ anode in solid oxide fuel cell stack after long-term operation," presented at the 12th Eur. SOFC SOE Forum, 2016, pp. 1–10.
[39] N. Vivet *et al.*, "Effect of Ni content in SOFC Ni-YSZ cermets: A three-dimensional study by FIB-SEM tomography," *J. Power Sources*, vol. 196, no. 23, pp. 9989–9997, Dec. 2011.
[40] V. Kachitvichyanukul, "Comparison of three evolutionary algorithms: GA, PSO, and DE," *Ind. Eng. Manage. Syst.*, vol. 11, no. 3, pp. 215–223, Sep. 2012.
[41] K. F. Man, K. S. Tang, and S. Kwong, "Genetic algorithms: Concepts and applications [in engineering design]," *IEEE Trans. Ind. Electron.*, vol. 43, no. 5, pp. 519–534, Oct. 1996.
[42] D. E. Goldberg, *Genetic Algorithms in Search, Optimization and Machine Learning*. Boston, MA, USA: Addison-Wesley, 1989.
[43] J. Kennedy and R. Eberhart, "Particle swarm optimization," in *Proc. IEEE Int. Conf. Neural Netw. (ICNN)*, Perth, WA, Australia, vol. 4, Nov./Dec. 1995, pp. 1942–1948.
[44] Y. Shi and R. Eberhart, "A modified particle swarm optimizer," in *Proc. IEEE Int. Conf. Evol. Comput.*, Anchorage, AK, USA, May 1998, pp. 69–73.
[45] D. L. Cavalca and R. A. S. Fernandes, "Gradient-based mechanism For PSO algorithm: A comparative study on numerical benchmarks," in *Proc. IEEE Cong. Evol. Comput. (CEC)*, Rio de Janeiro, Brazil, Jul. 2018, pp. 1–7.
[46] M. Qais and Z. AbdulWahid, "A new method for improving particle swarm optimization algorithm (TriPSO)," in *Proc. 5th Int. Conf. Modeling, Simulation Appl. Optim. (ICMSAO)*, Hammamet, Tunisia, Apr. 2013, pp. 1–6.

SZYMON BUCHANIEC received the B.S. and M.S. degrees in energy engineering from the AGH University of Science and Technology (AGH UST), Kraków, in 2017 and 2018, respectively, where he is currently pursuing the B.S. degree in applied computer science and the Ph.D. degree in energy engineering. His recent research interest includes effective and modern programming and their application in physics.

ANNA SCIAZKO received the Ph.D. degree (Hons.) from the Faculty of Energy and Fuels, AGH University of Science and Technology, Kraków, Poland, and the Shibaura Institute of Technology, Tokyo, Japan, in 2016, through the Double Diploma Program. She is currently an Assistant Professor with the AGH University of Science and Technology. She successfully continued her research under JSPS Postdoctoral Research Fellowship at the Institute of Industrial Science, The University of Tokyo, Tokyo. She also studied energy-related subjects at research institutions, such as the University of Iceland, Reykjavik, Iceland, and the École Polytechnique Fédérale de Lausanne, Lausanne, Switzerland. Her current research interests include experimental and numerical studies on fuel cells and energy systems.

MARCIN MOZDZIERZ received the Ph.D. degree (Hons.) from the Faculty of Energy and Fuels, AGH University of Science and Technology, Kraków, Poland, and the Shibaura Institute of Technology, Tokyo, Japan, in 2019, through the Double Diploma Program. He is currently an Assistant Professor with the Department of Fundamental Research in Energy Engineering, AGH University of Science and Technology. His research interests include solid oxide fuel cell technology, steam reforming of hydrocarbon fuels, mathematical and numerical modeling of physical phenomena, and high-performance computing.

GRZEGORZ BRUS received the Ph.D. degree (Hons.) from the Faculty of Energy and Fuels, AGH University of Science and Technology, Kraków, Poland, in 2011. He conducted the experimental part of his Ph.D. program under the bilateral agreement at the Shibaura Institute of Technology, Tokyo, Japan. He spent two successive years at the Department of Aeronautics and Astronautics, Kyoto University, Japan. He also studied energy-related subjects at research institutions, such as the University of Twente, Enschede, The Netherlands, and the École Polytechnique Fédérale de Lausanne, Lausanne, Switzerland. He is currently an Assistant Professor with the Department of Fundamental Research in Energy Engineering, AGH University of Science and Technology, where he is leading the project Easy-to-Assemble Stack Type (EAST): Development of Solid Oxide Fuel Cell Stack for the Innovation in the Polish Energy Sector, financed by the Foundation for Polish Science and co-financed by the European Union under Regional Development Founds. He has authored or co-authored over 75 papers in journals and international conferences. His current research interests include mathematical modeling, evolutionary computing, multi-objective optimization, and artificial neural networks and their applications in distributed energy systems.